Physics of Plasmas ARTICLE scitation.org/journal/php

Microtearing instabilities and electron thermal transport in low and high collisionality NSTX discharges

Cite as: Phys. Plasmas **28**, 022504 (2021); doi: 10.1063/5.0029120
Submitted: 9 September 2020 · Accepted: 14 January 2021 ·
Published Online: 3 February 2021

T. Rafiq,[1,a)] S. Kaye,[2] W. Guttenfelder,[2] J. Weiland,[1] E. Schuster,[1] J. Anderson,[3] and L. Luo[1]

AFFILIATIONS

[1]Department of Mechanical Engineering and Mechanics, Lehigh University, Bethlehem, Pennsylvania 18015-3085, USA
[2]Princeton Plasma Physics Laboratory, Princeton, New Jersey 08543, USA
[3]Department of Space, Earth, and Environment, Chalmers University of Technology and EURATOM-VR Association, SE-41296 Gothenburg, Sweden

[a)]Author to whom correspondence should be addressed: rafiq@lehigh.edu

ABSTRACT

Microtearing mode (MTM) real frequency, growth rate, magnetic fluctuation amplitude, and resulting electron thermal transport are studied in systematic NSTX scans of relevant plasma parameters. The dependency of the MTM real frequency and growth rate on plasma parameters, suitable for low and high collision NSTX discharges, is obtained by using the reduced MTM transport model [T. Rafiq *et al.*, Phys. Plasmas **23**, 062507 (2016)]. The plasma parameter dependencies are compared and found to be consistent with the results obtained from MTM using the gyrokinetic GYRO code. The scaling trend of collision frequency and plasma beta is found to be consistent with the global energy confinement trend observed in the NSTX experiment. The strength of the magnetic fluctuation is found to be consistent with the gyrokinetic estimate. In earlier studies, it was found that the version of the multi-mode (MM) anomalous transport model, which did not contain the effect of MTMs, provided an appropriate description of the electron temperature profiles in standard tokamak discharges and not in spherical tokamaks. When the MM model, which involves transport associated with MTMs, is incorporated in the TRANSP code and is used in the study of electron thermal transport in NSTX discharges, it is observed that the agreement with the experimental electron temperature profile is substantially improved.

I. INTRODUCTION

The ability to understand the physics involved in fusion plasmas, and, in particular, transport, requires integrated predictive simulations where all the relevant interactive physics are included. The simulations need to be carried out for the duration of the existence of the plasma, that is, for time periods ranging from seconds to thousands of seconds. Thousands of processors, running for many days, are required to carry out a few microsecond simulation of plasma turbulence using gyrokinetic models. Therefore, it is not possible to carry out the required integrated simulations using first-principles physics. Consequently, it is of the utmost importance to have fluid or unified fluid/kinetic physics-based reduced transport models that can be utilized in integrated physics simulations.

Microtearing mode (MTM)-induced turbulence has been reported to make a major contribution to electron thermal transport in standard and spherical tokamak discharges.[1–28] MTMs are kinetic extension of magnetohydrodynamic (MHD) tearing modes. MTMs are usually electromagnetic in character, and in the presence of collisionality, they are driven by electron temperature gradient. Electromagnetic MTMs propagate in the direction of electron diamagnetic drift. In contrast to electron temperature gradient-driven modes, which are electron scale or sub-ion scale modes, MTMs are short wavelength ion scale modes. It has been suggested that the component of fluctuating magnetic field in the direction of electron temperature gradient drives current that can turn microtearing modes unstable. In the previous publications,[4,11,12,29,30] the magnetic fluctuations due to microtearing turbulence are obtained using a quasi-linear estimate of saturated amplitudes to be $\delta B = B\rho_e/L_{Te}$, where ρ_e is the electron gyroradius and L_{Te} is the electron temperature gradient scale length. However, an improved saturation rule for microtearing mode was derived,[31] which indicated the dependence of the magnetic fluctuation on other parameters such as density gradient, plasma beta, wavenumber, field line bending, and collisionality. A reduced model for MTMs was developed[31] for the multi-mode (MM) anomalous transport

model[32] and incorporated into the time-dependent tokamak transport and data analysis code, TRANSP.[33] The aim of developing MTM model is to enhance the prediction of electron thermal transport induced by microtearing mode turbulence and, consequently, prediction of electron temperature profile in tokamak scenarios where MTMs are unstable. The developed MTM model improves the older slab theory by treating arbitrary electron collisionality and incorporating magnetic curvature effects. The reduced MTM model has been shown to replicate many of the linear gyrokinetic findings predicted in NSTX discharges, such as variations in real frequency and growth rates with poloidal wavenumber, beta, and electron temperature gradients.

The ion thermal confinement in NSTX plasmas is routinely similar to neoclassical levels in beam-heated H-mode plasmas, while the thermal electron transport is the dominant channel of power loss and remains relatively poorly understood and may restrict the global scaling of energy confinement.[34] Gyrokinetic simulations have shown that MTMs are capable of driving substantial thermal electron transport at levels that match those indicated by NSTX high-collision experiments.[18]

We make six particularly significant changes in this work compared to the paper published on DIII-D like conventional tokamak data:[35] (1) the data for low aspect ratio tokamak NSTX is used to calculate the MTM real frequency, growth rate, perturbation of the magnetic field, and thermal diffusivity of the electron; (2) the real frequency and growth rate of the reduced MTM model as a function of the plasma parameters are contrasted with the corresponding gyrokinetic results; (3) the high β_e NSTX results are compared and contrasted with the low β_e DIII-D results; (4) the variations of saturated amplitude with plasma beta, density gradient, and temperature gradient are demonstrated; (5) the reduced MTM model is included in the multi-mode anomalous transport module[32] and is installed in the integrated modeling TRANSP code to carry out electron temperature prediction for low and high collisionality NSTX discharges; and (6) the predicted electron temperature results are compared with corresponding low and high collisionality NSTX experimental data.

In Section II, the MTM reduced transport model, developed in Ref. 31, is briefly described. In Section III, the MTM linear stability dependency on plasma parameters, appropriate for NSTX discharges, is obtained employing the reduced MTM transport model. The dependencies on plasma parameters are compared with corresponding results of microtearing mode obtained from simulations of the first-principle gyrokinetic code GYRO.[36] In Section IV, the detailed scans are carried out to show the linear stability of MTM on NSTX plasma parameters. In Section V, the dependence of the magnetic fluctuation amplitude on different plasma parameters is shown. In Section VI, the variance of real frequencies, growth rates, magnetic fluctuations, and thermal electron diffusivities with NSTX plasma profiles are shown. In Section VII, predictive simulations of the electron temperature profiles for low and high collisionality NSTX plasmas are presented with and without including a component of the MTM reduced transport model in the TRANSP code. Section VIII summarizes the results of microtearing modes in NSTX discharges.

II. NONLINEAR MICROTEARING MODE TRANSPORT MODEL

Equation (1) of Ref. 35 in the linear limit is utilized to compute the MTM eigenvalues. The MTM electron thermal diffusivity is computed using the dependence of diffusivity on the magnetic correlation length, according to the Rechester–Rosenbluth model, given by

$$\chi_e = L_c u_{th}^2 \frac{|\delta B|^2}{B^2}, \tag{1}$$

where L_c represents a decorrelation length in collisionless and collisional limits.

In collisionless limit ($\lambda_{MFP} = u_{th}/\nu_e > qR$),

$$L_c = qR$$

and in the collisional limit ($\lambda_{MFP} < qR$),

$$L_c = u_{th}/\nu_e.$$

The magnetic field fluctuation amplitude, $\delta B/B$, is determined using the non-linear electromagnetic microtearing mode equation Eq. (4) of Ref. 35 as the driving force of microtearing instability. It is worth mentioning here that the model Rechester–Rosenbluth used to measure the heat diffusivity of electrons in stochastic magnetic fields might overestimate the transport of electron heat if kinetic effects are considered, as shown in kinetic simulations by Park *et al.*[37] This is especially important in a regime of low collisionality.

In Section III, it is shown that physics-based MTM reduced transport model is capable of reproducing the trends predicted by first-principles gyrokinetic simulations.[38]

III. COMPARISON OF RESULTS OBTAINED USING MTM REDUCED TRANSPORT MODEL AND THE GYROKINETIC CODE GYRO

The real frequencies and growth rates of reduced MTM model are compared with the corresponding values of the gyrokinetic code GYRO.[36] The linear GYRO scans were published in Ref. 38. The plasma parameter values corresponding to the NSTX discharge 120968 are used to obtain the results. This shot is a part of the dimensionless collisionality ν^* and the plasma beta β confinement scaling studies.[34] The plasma parameters are: the major radius $R = 0.94$ m, the minor radius $a = 0.62$ m, the radius of a local magnetic surface $r_{min} = 0.37$ m, the toroidal magnetic field strength $B_T = 0.35$ T, the electron beta $\beta_e = 0.09$, the safety factor $q = 1.7$, the magnetic shear $\hat{s} = 1.7$, the electron temperature $T_e = 0.45$ keV, the poloidal to the radial wavenumber $k_y/k_x = 0.2$, the electron density $n_e = 6.0 \times 10^{19}$ m^{-3}, the ratio of the major radius to the electron temperature, and density scale lengths $g_{Te} = R/L_{Te} = 4.1$ and $g_{ne} = R/L_{ne} = 0$.

The normalized growth rate ($\gamma a/c_s$) and the normalized real frequency ($\omega_r a/c_s$) of the most unstable MTM as a function of the normalized poloidal wavenumber, $k_y\rho_s$, are shown in Fig. 1. Results obtained using the first-principle gyrokinetic model are indicated by a circle-dashed line, and the results of the reduced MTM model are indicated by a square-dashed line. A good agreement is achieved with the MTM results obtained using the gyrokinetic code GYRO. The large and small values of $k_y\rho_s$ are found to be stabilizing. The fastest mode growth rate of MTM is found to be around $k_y\rho_s = 0.67$, and the magnitude of the corresponding mode frequency is around 200 kHz. This result indicates that the wavelength of MTM in NSTX plasma is greater than the wavelength of the electron temperature gradient mode but it is smaller than the wavelength of the ion temperature gradient (ITG) mode. Note in conventional low beta DIII-D tokamak plasmas, the fastest growing MTM was found to be around

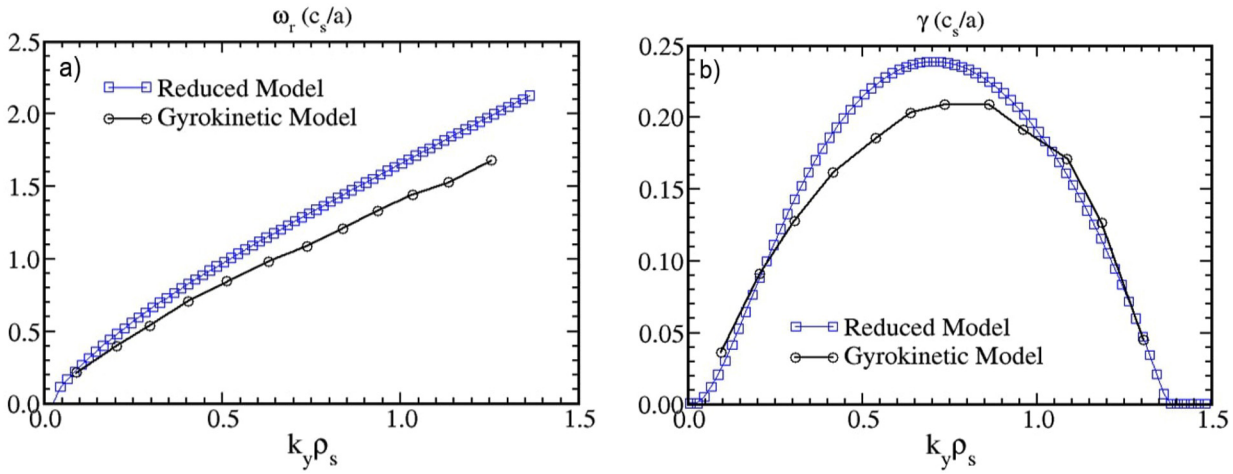

FIG. 1. (a) The linear frequency, $\omega_r a/c_s$, and (b) growth rate, $\gamma a/c_s$, is plotted as $k_y\rho_s$ function. The square dashed lines are the result from a reduced microtearing mode model and the circle dashed lines are the result from a first-principle gyrokinetic code GYRO. The maximum MTM growth rate in $k_y\rho_s$ spectrum is found to be around $k_y\rho_s = 0.67$, while the growth rate vanishes for $k_y\rho_s > 1.4$ due to linear FLR stabilization and toroidal effects in the NSTX H-mode discharge 120968.

$k_y\rho_s = 0.1$.[35] It indicates that ion temperature gradient and microtearing modes can coexist at similar wavelengths in low β_e tokamak plasmas. However, ITG modes propagate in the direction opposite to the direction of MTMs. The MTM real frequency increases linearly with $k_y\rho_s$, indicating that MTM not only depends on electron diamagnetic drift frequency but also propagates in the electron diamagnetic drift direction and therefore is an electron mode.

Notice that the MTM derivation involves both electrostatic and electromagnetic potentials. The electromagnetic component of MTM is dominant and contributes significantly to NSTX discharges due to high-beta plasmas, while DIII-D discharges are typically low-beta plasmas and thus the electrostatic component of MTM is likely to contribute to electron thermal transport. In addition, in comparison to NSTX discharges, the microtearing modes in DIII-D discharges are longer wavelength modes and may have a stabilizing effect on MTM in DIII-D discharges due to flow shear.

Figure 2 indicates real frequencies and growth rates of MTM vs $k_y\rho_s$ for gyro-kinetic and reduced transport models as the electron temperature gradient (g_{Te}) is varying from 0.7 to 1.5× of NSTX data. The maximum growth rate and its corresponding frequency is found to increase with g_{Te}. Moreover, the location and magnitude of the fastest growing microtearing mode are found to be increasing with g_{Te}, which is successfully captured by the reduced MTM model. The fastest growing MTM modes are found to be around $k_y\rho_s \approx 0.4 - 0.8$, which indicates that MTM is ion scale short wavelength instability, that is, destabilized by the g_{Te}.

In Fig. 3, reduced model MTM linear real frequency and growth rate vs β_e are compared with the gyrokinetic code GYRO linear real frequency and growth rate. The MTM growth rate increases with an increase in β_e for low values and then saturates with an increase in β_e for higher values. The rise in the β_e value increases the electromagnetic fluctuation by the law of Ampère's, which increases the growth rate of MTM. However, due to the stabilizing effect of the finite Larmor radius and collisionality, the MTM is weakened at a very high beta, at a given temperature gradient, and thus, the growth rate of MTM is either decreased or saturated. The real frequency is noticed to be almost independent of β_e in both the reduced and gyrokinetic simulations. The MTM instability threshold in electron beta is found to be around $\beta_e = 3.0\%$, while the local experimental value of electron beta is 9.0%. The nonzero value of β_e for the mode to be unstable indicates that the MTM is electromagnetic mode. The modest electron beta destabilization for NSTX experimental values is consistent with a $\Omega\,\tau_E = \beta^{-0.1}$ energy confinement scaling in the NSTX experiment.[34]

The influence of collision frequency on real frequency and growth rate of the electromagnetic MTM mode is seen in Fig. 4. Real frequency and growth rate of the reduced MTM model are compared with the linear MTM real frequency and growth rate of the gyrokinetic code GYRO. The real frequency of MTM is found to be increasing with collision frequency. The maximum growth rate is found for intermediate values of collision frequency. The nonmonotonic dependence of growth rate on ν_{ei} is consistent with gyrokinetic simulations (see Fig. 5 of Ref. 18). However, the cutoff in growth rate for large values of ν_{ei} is found earlier in the reduced model as compared to the gyrokinetic results, which may be due to the disparity between the collision models used in the reduced and gyrokinetic simulations. The full collision operator is used for gyrokinetic simulations, while the basic Spitzer collision formula is used for electron ion collisions in the reduced MTM model. The growth rate decreases with decreasing ν_{ei}, which is consistent with the dependence on collisionality found in the NSTX discharges.[34] The presence of MTM instability at a low collision frequency makes MTM relevant for electron thermal transport in ITER discharges. However, due to low collisionality in ITER discharges, MTM might not play a major role since the most unstable mode is found at the intermediate collision frequency.

In Fig. 5, the MTM eigenvalues vs safety factor are presented. Although the magnitude of linear real frequency and growth rate in reduced and gyrokinetic models are not very different, but the decreasing of growth rate for larger values of safety factor in the gyrokinetic model results is not captured by the reduced model. The safety factor in the reduced microtearing mode derivation enters in the estimation

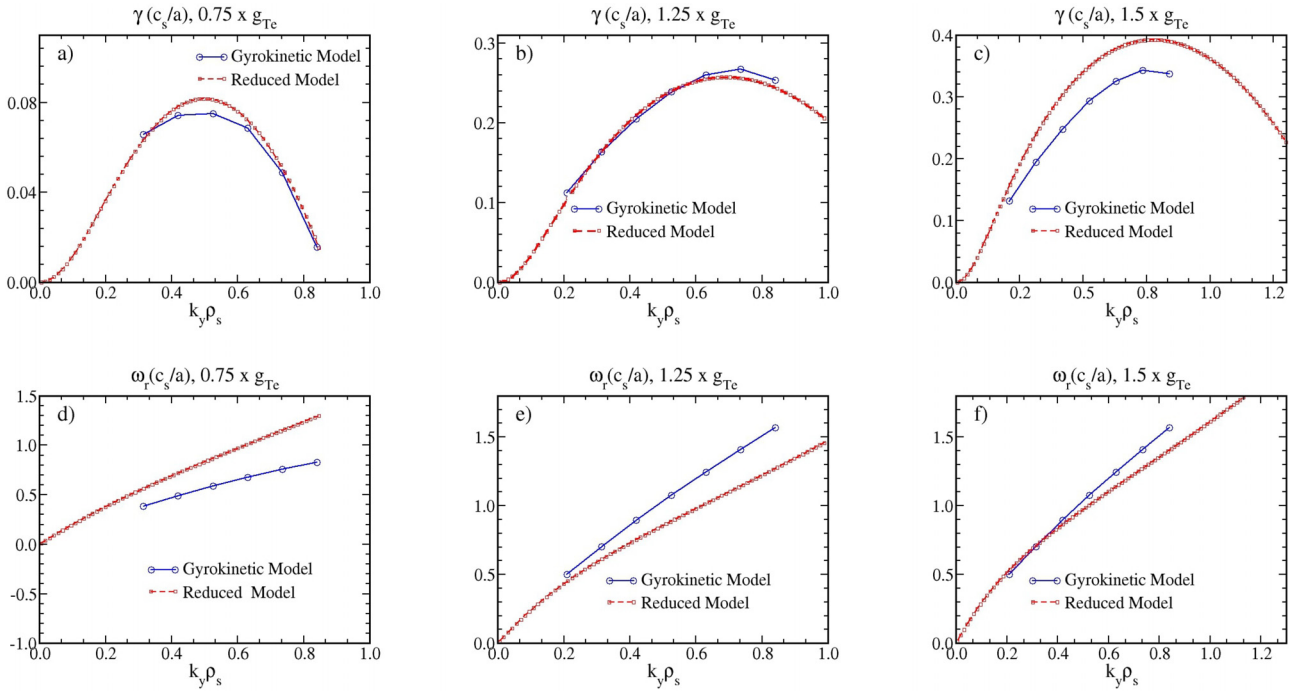

FIG. 2. [(a)–(c)] Growth rates, $\gamma a/c_s$ and [(d) and (e)] real frequencies, $\omega_r a/c_s$ are plotted vs $k_y\rho_s$ as normalized electron temperature gradient is varied over a range of 0.7–1.5× the NSTX data. Real frequency, growth rate, and position of the most unstable mode in the poloidal spectrum are increasing as the temperature gradient of the electron increases.

of parallel wavevector, $k_\parallel$, and in the average magnetic curvature formula. The simple estimation of parallel wavevector,[31] which does not depend on the toroidal geometry, might be a reason for not capturing the significant decreasing trend of growth rate for large values of the safety factor.

In short, there has been no physics-based reduced MTM transport model capable of reproducing the trends predicted by first-principles gyrokinetic simulations. A new unified fluid/kinetic model for microtearing modes has recently been developed that improves older slab theory by treating arbitrary electron collisionality and incorporating magnetic curvature effects. As a result, the reduced MTM model has been shown to replicate many of the linear gyrokinetic findings predicted in NSTX discharges, such as variations in real frequency and growth rates with poloidal wavenumber, beta, and electron

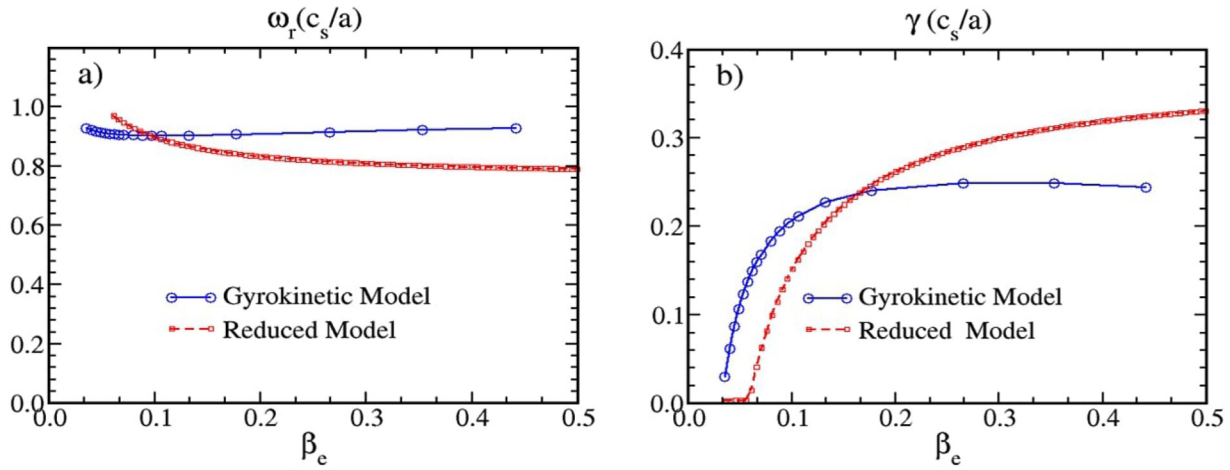

FIG. 3. (a) Real frequencies, $\omega_r a/c_s$, and (b) growth rates, $\gamma a/c_s$, are plotted as a function of β_e. The real frequencies are independent of β_e. Instability threshold in β_e is evident.

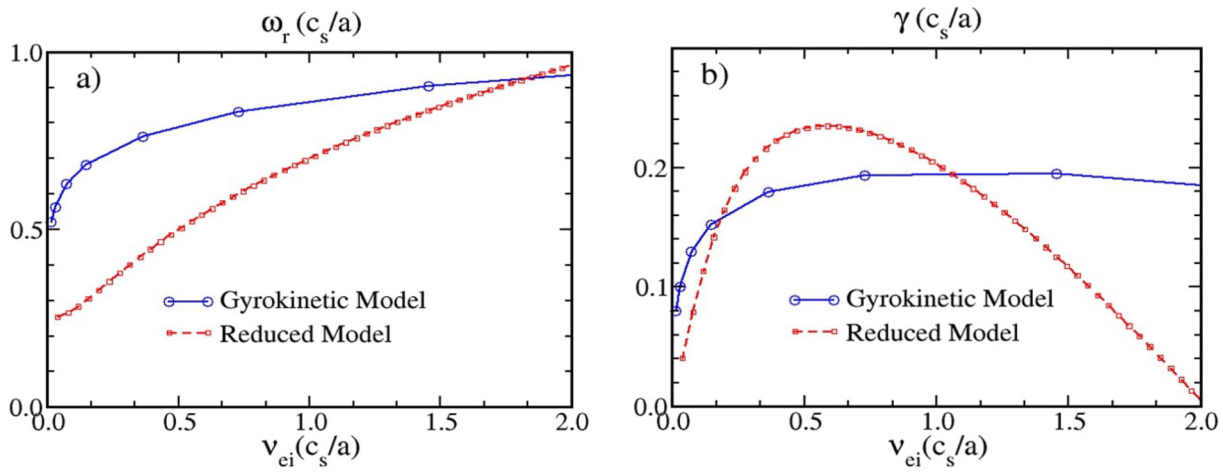

FIG. 4. (a) Real frequencies, $\omega_r a/c_s$, and (b) growth rates, $\gamma a/c_s$, are plotted as the normalized frequency of collision, $\nu_{ei} a/c_s$ function. The most unstable mode is at the intermediate collision frequency.

temperature gradients. One particularly significant finding is that the model recovers with collision frequency of the non-monotonic dependency of linear MTM growth rate.

IV. LINEAR STABILITY OF ELECTROMAGNETIC MTM ON NSTX PLASMA PARAMETERS

A detailed analysis of linear real-frequency and growth rate variation of electromagnetic microtearing mode on NSTX plasma parameters is seen using the reduced MTM model. Linear electromagnetic MTM stability on normalized temperature gradient, normalized poloidal wavenumber, normalized density gradient, and normalized collision frequency is presented.

In Fig. 6, microtearing mode linear real frequencies and growth rates are shown using the reduced MTM model as a function of g_{Te} for three different normalized gradient values of the electron density. Both the growth rates and associated frequencies increase with increasing the g_{Te}. The non-zero electron temperature gradients are found to be necessary for microtearing mode instability. The threshold of microtearing instability in the gradient of the electron temperature and the magnitude of the real frequency increase as the gradient of the electron density increases, while the growth rate declines at greater values of the normalized gradient of density. However, moderate increase in normalized density gradient has no effect on MTM growth rate. The NSTX experimental value of electron temperature gradient of microtearing mode is larger than the inferred linear threshold found in Fig. 6. Moreover, in contrast to low-β_e DIII-D discharge,[35] lower microtearing instability threshold in g_{Te} is found for high-β_e NSTX discharge.

In Fig. 7, the linear stability of MTM modes vs $k_y\rho_s$ is shown for three different values of $\eta_e (\equiv g_{Te}/g_{ne}) = 3.4, 5.1,$ and 6.8. The most

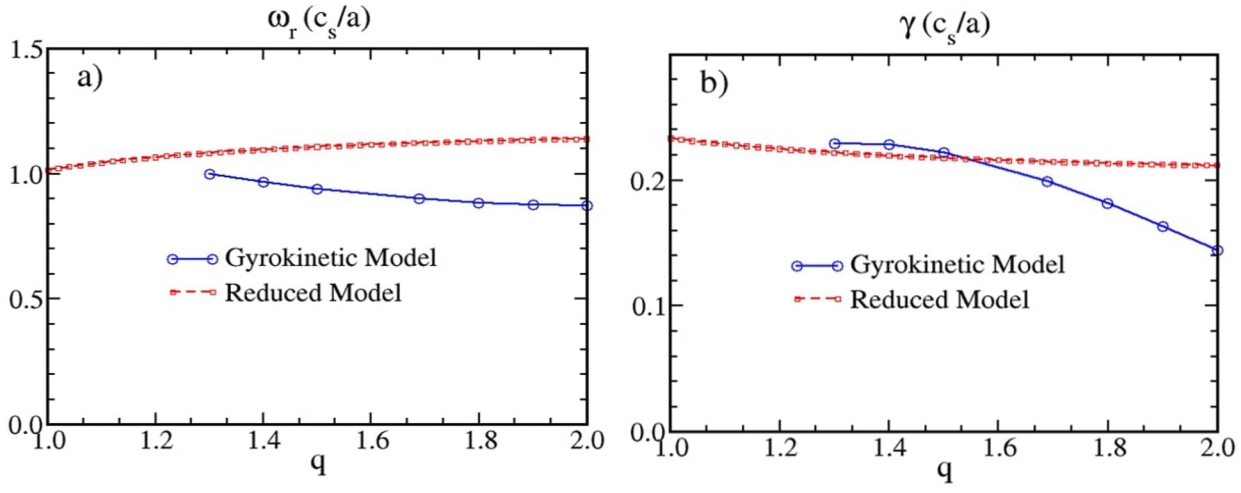

FIG. 5. (a) Real frequencies, $\omega_r a/c_s$, and (b) growth rates, $\gamma a/c_s$, are plotted as a safety factor q function. The decrease in growth rate for large values of safety factor is not captured by the reduced model.

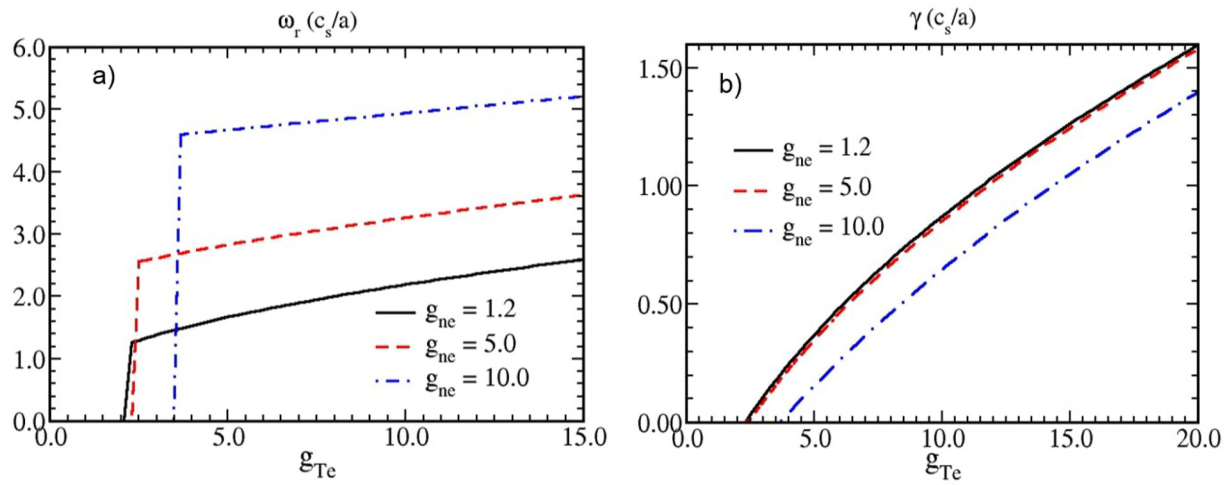

FIG. 6. (a) The linear real frequencies, $\omega_r a/c_s$, and (b) growth rates, $\gamma a/c_s$, vs temperature gradient g_{Te} are plotted for normalized density gradient, $g_{ne} = 1.2$, $g_{ne} = 5.0$, and $g_{ne} = 10$. Critical electron temperature gradient is required for microtearing instability to occur. The critical gradient decreases with decreasing density gradient.

unstable modes are found to be around $k_y\rho_s \approx 0.6 - 0.9$, which indicates that microtearing is shorter wavelength instability than ion temperature gradient mode in NSTX plasmas. The magnitude of the most unstable mode is found to increase with increasing η_e. The modes are found to be stabilizing for both small and large values of $k_y\rho_s$. The large values of η_e is destabilizing for both short and long wavelengths. The real frequency is in the direction of electron drift, which is found to increase with $k_y\rho_s$ increasing and with η_e increasing.

In Fig. 8, MTM modes as a function of $k_y\rho_s$ for flat ($g_{ne} = 0.0$), hallow ($g_{ne} = -1.2$), and normal ($g_{ne} = 1.2$) normalized density gradients are plotted. The hallow density profile is found to be the least MTM unstable, the normal density profile is the most unstable, and the flat density profile is intermediately unstable. In general, the growth rate of MTM does increase with increasing normalized density gradient at a fixed value of g_{Te}. The peaked value of the MTM mode is found to be around $k_y\rho_s \approx 0.65$. The location of the peaked value of the MTM mode in the $k_y\rho_s$ spectrum is not found to be changed with varying density gradient. However, with increasing g_{ne} and increasing wavenumber $k_y\rho_s$, the real frequency increases.

In Fig. 9, the normalized real frequency of the most unstable microtearing mode and corresponding growth rate is seen vs normalized density gradient, g_{ne}. The real frequency is increased with increasing gradient of density. The maximum growth rate is observed for the intermediate density gradient value $g_{ne} \simeq 2.2$. Both small and large values of density gradient are found to be stabilizing. The large density gradient $g_{ne} = 12$ stabilizes the microtearing mode completely. The density profile in the core of NSTX discharges is flat, so less stabilization is expected in the experiments from density gradient. It is

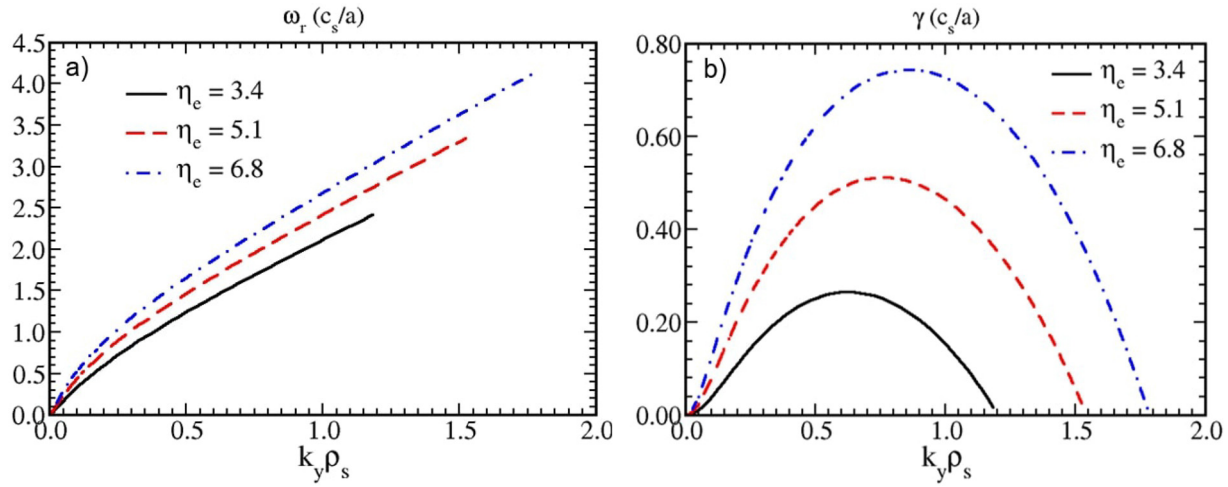

FIG. 7. (a) Real frequencies, $\omega_r a/c_s$, and (b) growth rates, $\gamma a/c_s$, vs $k_y\rho_s$ are shown for $\eta_e = 3.4$, 5.1, and 6.8. MTMs are shorter wavelength instability than ITG instability in NSTX plasmas.

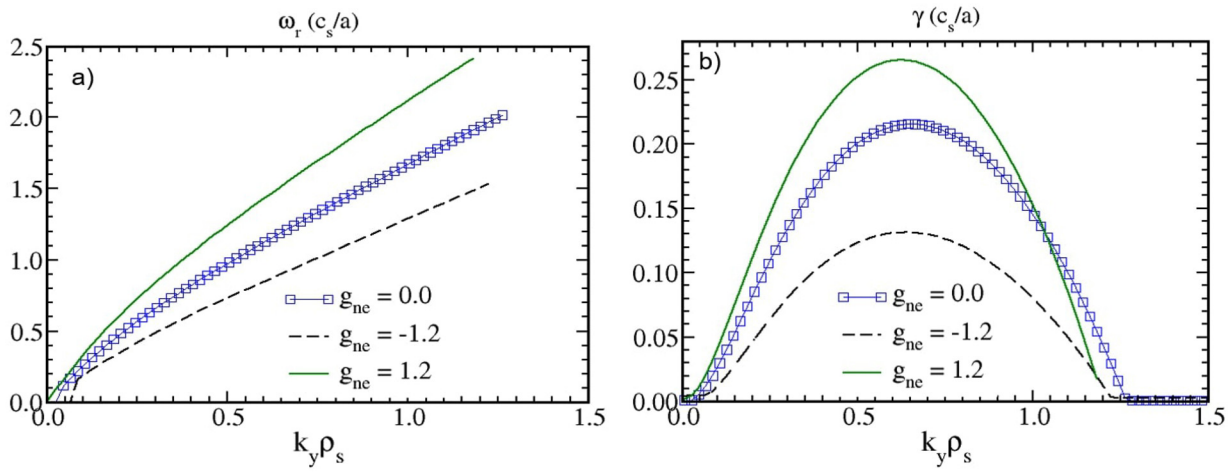

FIG. 8. (a) The variation of real frequencies, $\omega_r a/c_s$, and (b) growth rates, $\gamma a/c_s$, are plotted as a function of $k_y\rho_s$ for $g_{ne} = 0.0, -1.2,$ and 1.2. The hollow density profile is found to be least unstable.

worthwhile to mention here that density gradient was found to be destabilizing in low β_e DIII-D parameters.[35]

The normalized growth rate vs $Z_{eff}\nu_{ei}/\omega_r$ is plotted in Fig. 9. It is found that as collision frequency decreases, the MTM growth rate decreases as well. This may be in part is responsible for setting the favorable dimensionless energy confinement scaling, $\Omega\tau_E = \nu_*^{-0.8}$ found in NSTX H-mode discharges.[34] This behavior is in contrast to drift-type modes, where collisionality appears to have a stabilizing effect on trapped electron modes, which contrarily increase the electron and ion temperature gradient instability in the collisionless limit. The peak MTM growth rate occurs around $Z_{eff}\nu_{ei}/\omega_r \approx 2.0$. A slight shift in the peak value toward large collisionality is found when magnetic curvature, ω_{De}, is ignored. In Fig. 10(b), the assumption that $k_y\rho_s = 0.67$ for each value of ν_{ei} will remain fixed is relaxed and computation over $k_y\rho_s$ is accomplished to identify the value of the normalized poloidal wavenumber related to the fastest growing microtearing instability. In comparison to the fixed $k_y\rho_s$, the peak MTM growth rate occurs around $Z_{eff}\nu_{ei}/\omega_r \approx 1.0$ instead $Z_{eff}\nu_{ei}/\omega_r \approx 2.0$. The magnitude of the peak growth rate is also found to be large in case of varying wavenumber $k_y\rho_s$.

V. MAGNETIC FLUCTUATION DEPENDENCE ON ELECTRON BETA, TEMPERATURE GRADIENT, AND DENSITY GRADIENT

MTMs are unstable due to magnetic fluctuations that cause the formation of small magnetic island chains near the rational magnetic surfaces. The magnetic field lines break up and reconnects due to a narrow current layer near the rational magnetic surfaces. MTM model solves a nonlinear microtearing mode envelope equation [Eq. (55) of Ref. 31] that self-consistently determines an estimated saturated magnetic field fluctuation amplitude, $\delta B/B$. Our nonlinear saturation of the MTM instability is quite similar to that of Drake *et al.*[4] It is due to

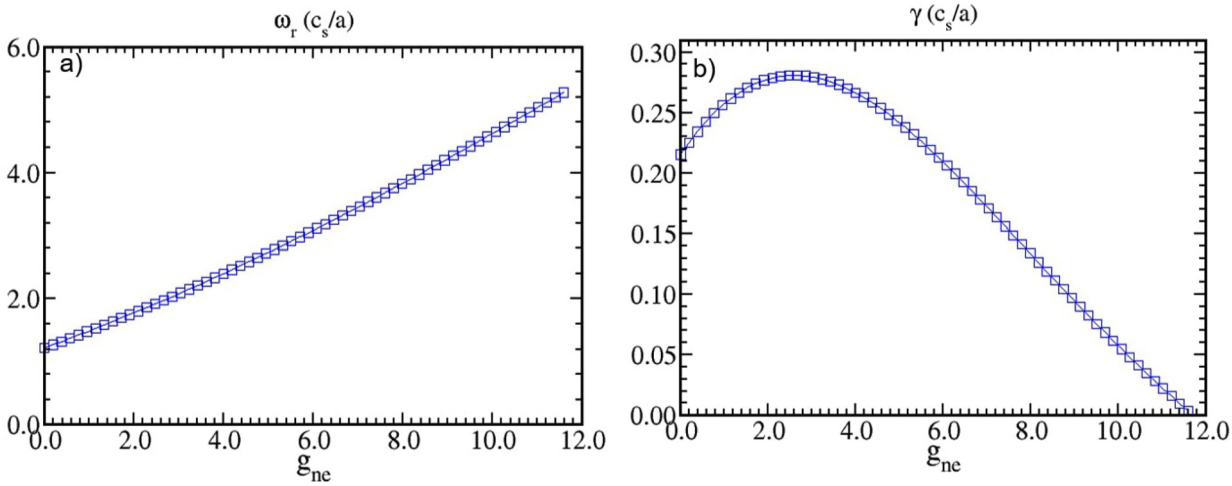

FIG. 9. (a) The variation of real frequencies, $\omega_r a/c_s$, and (b) linear growth rates, $\gamma a/c_s$, vs normalized density gradient, g_{ne}. Large density gradient is stabilizing.

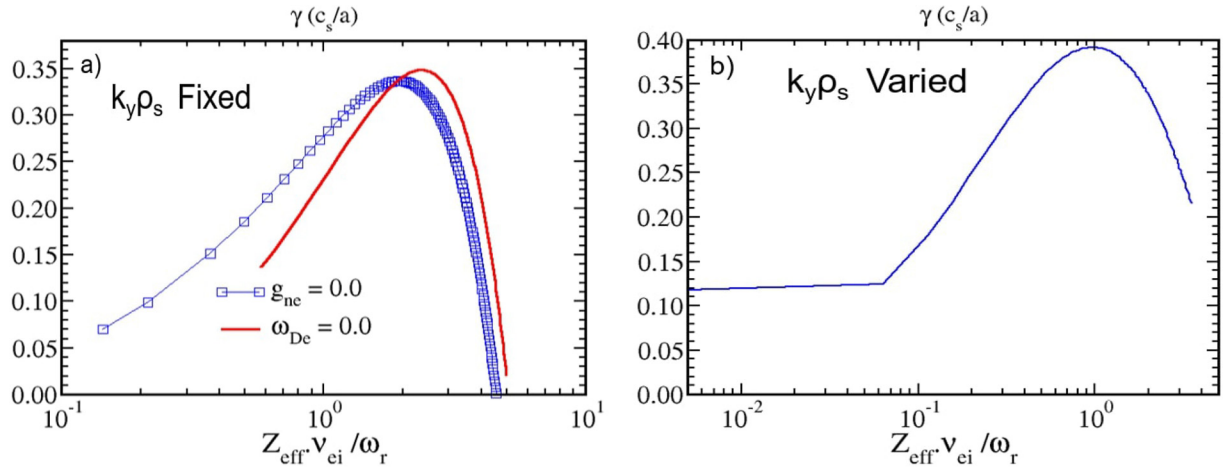

FIG. 10. (a) Linear growth rates, $\gamma a/c_s$ vs $Z_{eff}\nu_{ei}/\omega_r$ for fixed $k_y\rho_s$ and (b) for varying $k_y\rho_s$ are plotted. The square dashed curve is for $g_{ne} = 0$ and $\omega_{De} \neq 0$, while the solid curve is for $g_{ne} = 0$ and $\omega_{De} = 0$. Growth rate decreases with decreasing collisionality.

a cubic nonlinearity stemming from a nonlinear kink term. Our interpretation is also close to that of Drake *et al.* although we have here entered effects of line bending ($k_\parallel$) and toroidicity (ω_D). In the collision dominated limit, we find that the system approaches an electrostatic limit where transport would vanish. Thus, the collision frequency enters in the denominator. Note that the choice of collision term could be important. The effect of line bending enters primarily in the linear eigen-frequency while toroidicity enters as a fluid resonance. We have seen for drift waves that this resonance is of a fluid nature.[39]

The dependence of $\delta B/B$ on β_e, normalized temperature gradient, g_{Te}, and normalized density gradient, g_{ne}, is plotted in Fig. 11. The magnetic fluctuation amplitude clearly shows dependence on β_e, temperature and density gradients. The magnetic fluctuation amplitude is found to increase with increase in β_e, temperature, and density gradient. An increase in magnetic fluctuation indicates that electron turbulence and electron thermal transport driven by microtearing mode will increase with increasing β_e, g_{Te}, and g_{ne}. *In prior* MTM publications,[4] microtearing instability is believed to saturate when the magnitude of the magnetic field fluctuation is equal to the ratio of the electron Larmor radius, ρ_e, to the scale length, L_{Te}, of electron temperature gradient. This basic saturation rule is incapable of catching the dependencies of magnetic fluctuation seen in Fig. 11.

VI. BEHAVIOR OF MTM MODEL FOR NSTX PROFILES

In Fig. 12, the profiles and their gradients are shown for an NSTX tokamak discharge 120968. The growth rates, real frequency, and values of $k_y\rho_s$ associated with the fastest growing MTM mode are shown vs radius in Figs. 13(a)–13(c). The magnetic fluctuation amplitude, $\delta B/B$, and microtearing electron thermal diffusivity, $\chi_e(m^2/s)$, profiles are plotted in Figs. 13(d)–13(e). The microtearing mode is found to be linearly unstable at most radial locations. However, the growth rate is found to be larger in the radial locations of a large temperature gradient and found to be small in the radial locations of a small temperature gradient. A transition of mode frequency orientation is observed from the diamagnetic direction of the electron to the diamagnetic direction of the ion with a difference in the sign of the normalized density gradient. The values of $k_y\rho_s < 1.0$ over the whole plasma radius depict that the MTM is ion scale mode. The saturated amplitude of the magnetic field fluctuation is found $\delta B/B \approx 10^{-4} - 10^{-3}$, which is consistent with the gyrokinetic estimate of the magnetic fluctuation amplitude $\delta B/B \approx 8 - 9 \times 10^{-3}$ at $r/a = 0.6$, as reported in Fig. 4 of Ref. 38. The amplitude is based on the fastest growing mode, the real frequency, and sidebands in the normalized poloidal wavenumber spectrum. The χ_e based on $\delta B/B$ are found to be large in the vicinity of moderate collisionality in Fig. 13(e).

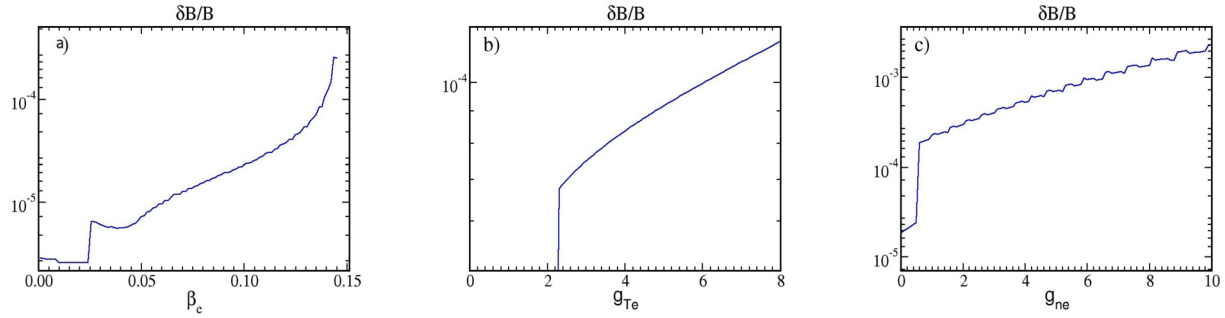

FIG. 11. Nonlinear calculation of magnetic fluctuation amplitude, $\delta B/B$, (a) vs β_e, (b) vs normalized temperature gradient, g_{Te}, and (c) vs normalized density gradient, g_{ne}.

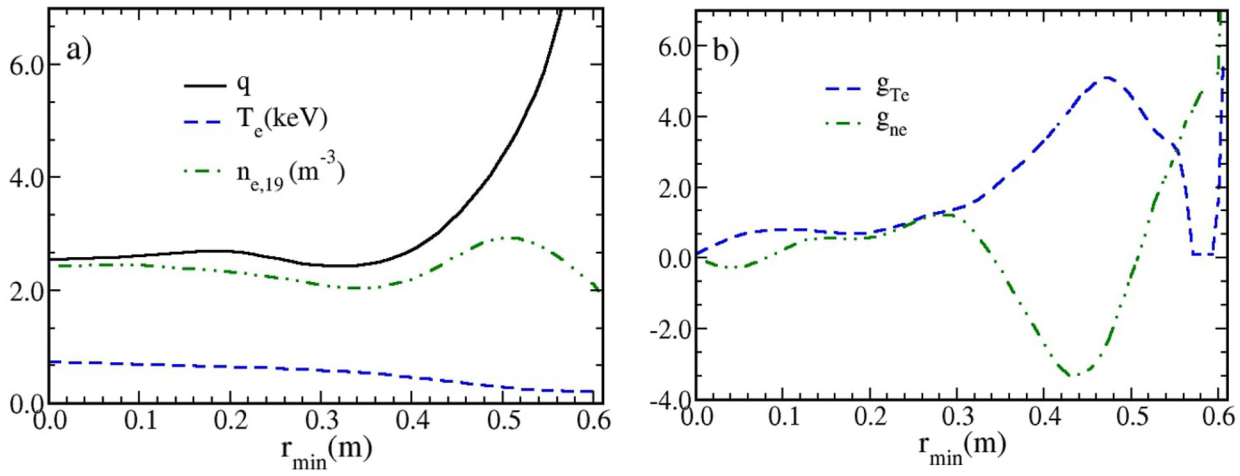

FIG. 12. (a) Radial profiles of q, T_e, and $n_{e,19}$ and (b) corresponding normalized temperature and density gradient profiles for the NSTX H-mode discharge.

The amplitude of magnetic fluctuations and the electron heat transport caused by microtearing mode turbulence are found to be small in the hollow density gradient region and they are found to be large at the plasma edge region due to a large value of normal density and temperature gradients. A pronounced electron temperature pedestal can be expected in the case of hollow density profiles at the tokamak edge due to decreasing microtearing mode driven electron thermal transport.

VII. PREDICTED AND MEASURED ELECTRON TEMPERATURE FOR A HIGH AND A LOW ν^* NSTX DISCHARGE

The multi-mode (MM) anomalous transport model[32] is a mixture of theory-based transport models. The development of the MM transport model is motivated by the fact that different derivations using different sets of approximations are used to estimate the transport from different kinds of instabilities, which may dominate in

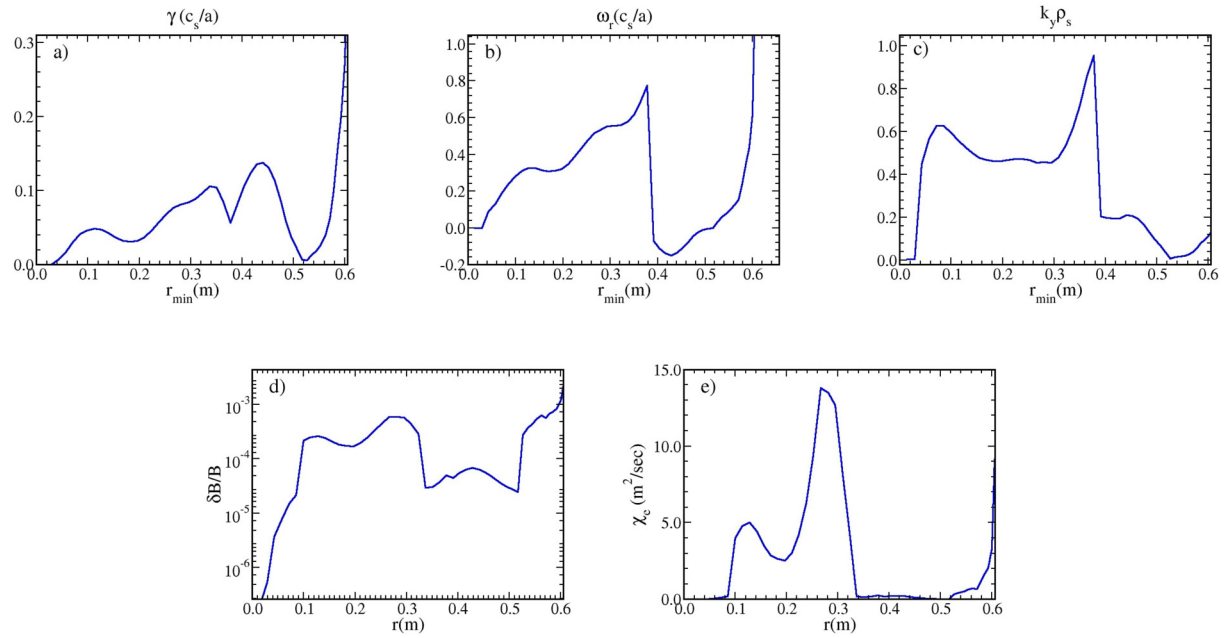

FIG. 13. (a) Linear growth rates, $\gamma a/c_s$, (b) real frequencies, $\omega a/c_s$, (c) corresponding values of normalized poloidal wavenumber $k_y\rho_s$, (d) magnetic fluctuation amplitude, $\delta B/B$, and (e) electron thermal diffusivity, χ_e are plotted vs NSTX minor radius in a collisional limit. In the hollow density gradient region, the magnetic fluctuation amplitude and the resulting electron thermal transport are observed to be small and are observed to be large at the plasma edge area due to high values of normal density and temperature gradients.

different parts of the plasma. Usually, the diffusivities from these independently derived transport models are added together and combined with the neoclassical transport. The MM is used to predict temperature, density, and rotation profiles for tokamak plasmas in integrated whole device modeling codes. The earlier version of the MM model contained contributions to electron thermal transport from the ion temperature gradient, trapped electrons, kinetic and resistive ballooning, peeling, collisionless and collision-dominated MHD modes, and electron temperature gradient modes. The newly developed MTM model[31] is used as part of the MM model to define the transport that has previously been omitted in the earlier version of the MM model. The current version of the MM transport model used in this study is formulated by combining transport from the earlier version of the MM model with transport from the reduced MTM model. The most fundamental difference between electron transport in previous MM and due to MTMs is that in MM electron thermal transport is due to $\mathbf{E} \times \mathbf{B}$ motion, while in MTMs, it is due to perturbations of the magnetic flux surfaces.

This research is aimed at understanding the evolution of the NSTX electron temperature profiles. A developed MTM model is incorporated into the MM anomalous transport model. The MM model is then implemented in the integrated modeling simulation code TRANSP. A comparison of the predicted electron temperature profiles using this model is shown for NSTX low and high collisionality H-mode discharges in Figs. 14(a) and 14(b). The electron collisionality as a function of the normalized poloidal flux is shown in Fig. 14(c). The boundary condition for predictive simulations is set at $\rho = 0.8$. In earlier studies, it was found that the MM transport model version, which did not have the effect of microtearing modes, provided an appropriate description of the electron temperature profiles in high-collisionality standard tokamak discharges.[40,41] When the MM model, which involves transport associated with microtearing modes, is installed in the TRANSP code and is used in the study of electron thermal transport in NSTX discharges, it is found, as shown in Fig. 14(a), that compliance with the experimental electron temperature profile is substantially improved in the high collision NSTX discharge 129016. As seen in Fig. 14(b), simulated electron temperature profiles are also compared with experimental electron temperature profiles for low collisionality NSTX 129039 discharge. The model is found to over-predict the transport at low collisionality, predicting lower electron temperature profile as compared to the corresponding experimental temperature profile. The RMS deviation from the experimental profile of the predicted electron temperature profile for low collisionality discharge is calculated to be 19%.

The different components of the MM model provide contributions to transport in the different regions of plasma discharge, as shown in Figs. 14(d) and 14(e) for high and low collisionality discharges. MTMs are found to be unstable in the entire confinement region ($0.2 \leq \rho \leq 0.8$) for high collisionality discharge, while they are mainly unstable in the region of $0.6 \leq \rho \leq 0.8$ for a low collisionality

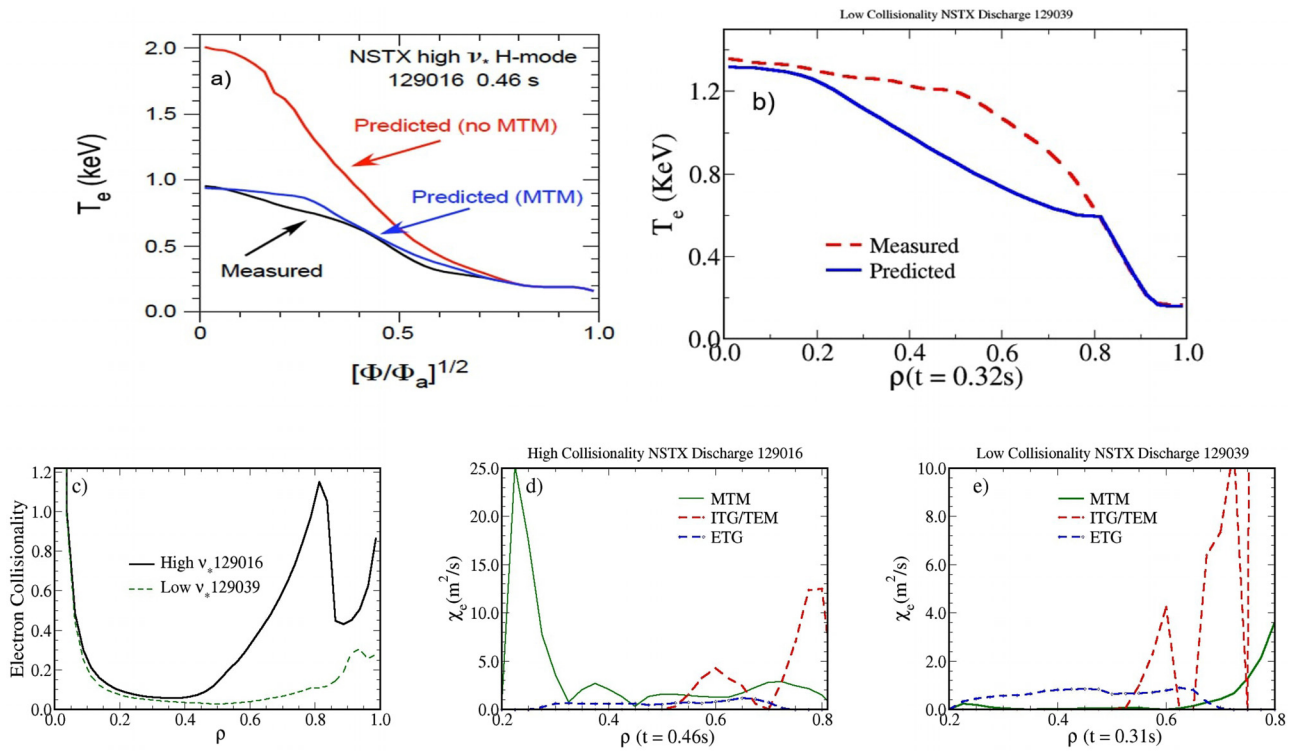

FIG. 14. (a) Simulated and experimental electron temperatures are plotted for the high ν^* NSTX discharge, 129016, with and without the transport contribution associated with microtearing modes, and (b) for the low ν^* NSTX discharge, 129039, [(c)–(e)] electron collisionality and components of electron thermal diffusivity for the low and high ν^* discharges depending on the normalized square root of the toroidal flux, ρ. The agreement with the experimental electron temperature profile is dramatically enhanced for high ν^* collision discharge. However, the model is found to over-predict transport for low ν^* discharge.

discharge. In addition, the magnitude of electron thermal diffusivity due to MTM is found to be large in the high collisionality discharge relative to low collisionality discharge. Diffusivity due to electron temperature gradient (ETG) modes is found to be similar in both discharges. However, the diffusivity due to ITG/TEM is found to be high in low collisionality discharge.

Transport due to ETG modes can be one of the potential explanations for not predicting an electron temperature profile for low ν^* discharge. Mainly, in both low and high collisionality discharges, diffusivity due to ETG modes is found to be similar. In earlier studies, the version of MM including the ETG model provided a suitable description of the electron temperature profiles in standard tokamak discharges. However, the MM module including ETG and MTM components under-predicts electron temperature profile (i.e., over-predicts electron thermal transport) in low-collisionality NSTX discharges. It has been found by NSTX experimentalists that: i—the rotation profile changes as collisionality varies, ii—the $\mathbf{E} \times \mathbf{B}$ flow shear can provide an effective suppression mechanism for ETG turbulence in NSTX deuterium H-mode discharges, and iii—reverse and low magnetic shear and density gradient can suppress electron thermal transport. Unfortunately, magnetic-shear, collisionality and $\mathbf{E} \times \mathbf{B}$ flow-shear effects are not included in the current version of the ETG model. The absence of these effects might explain why the expected reduction in electron thermal transport is not observed in low collisionality discharge. The other possibility that electron thermal transport is higher may be due to the ITG/TEM mode, which contributes to more transport than it should be. Future study will include improving the NSTX discharge electron thermal transport model for low-collisionality.

VIII. SUMMARY

The purpose of this research project is to illustrate the temporal evolution of NSTX H-mode low-and high-collision electron temperature profiles. Gyrokinetic calculations show that MTMs are a main source of electron thermal transport in these discharges. In order to understand the influence of MTMs on transport and, consequently, on the evolution of electron temperature in NSTX discharges, a reduced transport model for MTMs has recently been developed.[31] The dependency of MTM's real frequency and growth rate on NSTX plasma parameters achieved using a physics-based reduced model has been shown to be capable of reproducing the trends predicted by the first-principles gyrokinetic simulations. The temperature gradient along with the collision frequency and plasma beta was found to be adequate for MTM to become unstable in low-and high-collision NSTX discharges. It was shown that the model recovers the non-monotonic dependency of the MTM linear growth rate with the collision frequency. It was demonstrated that as collision frequency decreases, the MTM growth rate decreases as well. This trend is qualitatively consistent with the favorable global dimensionless energy confinement trend of $\Omega\,\tau_E = \nu^{*-0.8}$ in NSTX experiments. The weak dependence of MTM on β_e was also found to be qualitatively consistent with the observed NSTX trend, $\Omega\,\tau_E = \beta^{-0.1}$. The microtearing instability threshold was observed in electron temperature gradient and in β_e. The increase in the real frequency of MTM with increasing $k_y\rho_s$, temperature gradient, and density gradient showed drift nature of microtearing instability. Some properties of MTMs were found to be different in low β_e DIII-D discharges than those of the high β_e NSTX discharges. The MTM's saturated magnetic fluctuation strength and the corresponding electron thermal diffusivity were calculated. The calculation of magnetic fluctuation strength, $\delta B/B \approx 10^{-4} - 10^{-3}$, is found to be consistent with gyrokinetic estimation.

The significantly stronger magnetic field in DIII-D than in NSTX results in lower β_e and due to the fact that the highest MTM growth rate occurred at low perpendicular mode numbers of $k_y\rho_s \sim 0.1$, while in NSTX it was around $k_y\rho_s \sim 0.67$. The average curvature is expected to be smaller in DIII-D discharges due to the lower mode number and larger major radius. In addition, the parallel magnetic perturbation is expected to be smaller due to lower β_e. It is, therefore, likely that the MTM is a collisional slab like mode with a more destabilizing electrostatic contribution in DIII-D discharges. While the MTM is more likely to be a collisional curvature driven electromagnetic mode in NSTX discharges. Further, in the NSTX discharges, it was found that the rise in the beta value increases the electromagnetic fluctuation by the law of Ampère's, which increases the growth rate of MTM and the increase in MTM growth rate further increases the electromagnetic fluctuations. However, MTM is weakened at a very high beta due to the stabilizing effects of the finite Larmor radius and collisionality, at a given temperature gradient, and thus, the growth rate of MTM is either decreased or saturated.

The diffusivity is large in the regions of either moderate collisionality or large temperature gradients and is small in the region of hollow density gradient region. The MM module including the MTM model was installed in TRANSP and utilized to study electron thermal transport in low and high collisionality discharges in NSTX. The agreement with the experimental electron temperature profile is significant for high-collision discharges. But the MMM module tends to over-predict low-collisionality transport, predicting a lower profile of electron temperature.

ACKNOWLEDGMENTS

This work is supported by the U.S. Department of Energy, Office of Science, under Award Nos. DE-SC0013977, DE-FG02-92ER54141, and DE-AC02-09CH11466.

DATA AVAILABILITY

The data that support the findings of this study are available from the corresponding author upon reasonable request.

REFERENCES

[1]R. D. Hazeltine, D. Dobrott, and T. S. Wang, Phys. Fluids **18**, 1778 (1975).
[2]L. Chen, P. H. Rutherford, and W. M. Tang, Phys. Rev. Lett. **39**, 460 (1977).
[3]J. D. Callen, Phys. Rev. Lett. **39**, 1540 (1977).
[4]J. F. Drake, N. T. Gladd, C. S. Liu, and C. L. Chang, Phys. Rev. Lett. **44**, 994 (1980).
[5]A. B. Hassam, Phys. Fluids **23**, 2493 (1980).
[6]N. Ohyabu, G. Jahns, R. Stambaugh, and E. Strait, Phys. Rev. Lett. **58**, 120 (1987).
[7]J. Kesner and S. Migliuolo, Nucl. Fusion **39**, 163 (1999).
[8]C. M. Roach, D. J. Applegate, J. W. Connor, S. C. Cowley, W. D. Dorland, R. J. Hastie, N. Joiner, S. Saarelma, A. A. Schekochihin, R. J. Akers, C. Brickley, A. R. Field, M. Valovic, and MAST Team, Plasma Phys. Controlled Fusion **47**, B323 (2005).
[9]D. Applegate, C. Roach, J. Connor, S. Cowley, W. Dorland, R. Hastie, and N. Joiner, Plasma Phys. Controlled Fusion **49**, 1113 (2007).
[10]F. M. Levinton, H. Yuh, M. G. Bell, R. E. Bell, L. Delgado-Aparicio, M. Finkenthal, E. D. Fredrickson, D. A. Gates, S. M. Kaye, B. P. LeBlanc, R. Maingi, J. E. Menard, D. Mikkelsen, D. Mueller, R. Raman, G. Rewoldt, S. A.

Sabbagh, D. Stutman, K. Tritz, and W. Wang, Phys. Plasmas **14**, 056119 (2007).
[11]K. Wong, S. Kaye, D. Mikkelsen, J. Krommes, K. Hill, R. Bell, and B. LeBlank, Phys. Rev. Lett. **99**, 135003 (2007).
[12]K. L. Wong, S. Kaye, D. R. Mikkelsen, J. A. Krommes, K. Hill, R. Bell, and B. LeBlanc, Phys. Plasmas **15**, 056108 (2008).
[13]M. J. Pueschel, M. Kammerer, and F. Jenko, Phys. Plasmas **15**, 102310 (2008).
[14]D. R. Smith, W. Guttenfelder, B. P. LeBlanc, and D. R. Mikkelsen, Plasma Phys. Controlled Fusion **53**, 035013 (2011).
[15]W. Guttenfelder, J. Candy, S. M. Kaye, W. M. Nevins, E. Wang, R. E. Bell, G. W. Hammett, B. P. LeBlanc, D. R. Mikkelsen, and H. Yuh, Phys. Rev. Lett. **106**, 155004 (2011).
[16]D. Dickinson, C. M. Roach, S. Saarelma, R. Scannell, A. Kirk, and H. R. Wilson, Phys. Rev. Lett. **108**, 135002 (2012).
[17]S. Moradi, I. Pusztai, W. Guttenfelder, T. Fülöp, and A. Mollén, Nucl. Fusion **53**, 063025 (2013).
[18]W. Guttenfelder, J. Candy, S. M. Kaye, W. M. Nevins, E. Wang, J. Zhang, R. E. Bell, N. A. Crocker, G. W. Hammett, B. P. LeBlanc, D. R. Mikkelsen, Y. Ren, and H. Yuh, Phys. Plasmas **19**, 056119 (2012).
[19]C. C. Petty, W. Guttenfelder, C. Holland, S. Kaye, J. E. Kinsey, D. C. McDonald, G. R. McKee, L. Vermare, C. Angioni, C. Bourdelle, G. Hoang, F. Imbeaux, F. Ryter, H. Urano, and M. Valovic, in *Proceedings of the 24th International Conference on Fusion Energy* (IAEA, Vienna, San Diego, 2012), Paper No. ITR/P1-30.
[20]H. Doerk, F. Jenko, T. Görler, D. Told, M. J. Pueschel, and D. R. Hatch, Phys. Plasmas **19**, 055907 (2012).
[21]J. Canik, W. Guttenfelder, R. Maingi, T. Osborne, S. Kubota, Y. Ren, R. Bell, H. Kugel, B. LeBlanc, and V. Souhkanovskii, Nucl. Fusion **53**, 113016 (2013).
[22]S. M. Kaye, W. Guttenfelder, R. E. Bell, S. P. Gerhardt, B. P. LeBlanc, and R. Maingi, Phys. Plasmas **21**, 082510 (2014).
[23]D. Hatch, M. Kotschenreuther, S. Mahajan, P. Valanju, F. Jenko, D. Told, T. Görler, and S. Saarelma, Nucl. Fusion **56**, 104003 (2016).
[24]M. Kotschenreuther, D. Hatch, S. Mahajan, P. Valanju, L. Zheng, and X. Liu, Nucl. Fusion **57**, 064001 (2017).
[25]S. Maeyama, T.-H. Watanabe, and A. Ishizawa, Phys. Rev. Lett. **119**, 195002 (2017).
[26]X. Jian, C. Holland, J. Candy, E. Belli, V. Chan, A. M. Garofalo, and S. Ding, Phys. Rev. Lett. **123**, 225002 (2019).
[27]J. Chowdhury, Y. Chen, and S. E. Parker, Phys. Plasmas **27**, 042309 (2020).
[28]T. Xie, M. J. Pueschel, and D. R. Hatch, Phys. Plasmas **27**, 082306 (2020).
[29]R. R. Dominguez, M. Rosenberg, and C. S. Chang, Phys. Fluids **24**, 472 (1981).
[30]G. G. Craddock and P. W. Terry, Phys. Fluids B **3**, 3286 (1991).
[31]T. Rafiq, J. Weiland, A. H. Kritz, L. Luo, and A. Y. Pankin, Phys. Plasmas **23**, 062507 (2016).
[32]T. Rafiq, A. H. Kritz, J. Weiland, A. Y. Pankin, and L. Luo, Phys. Plasmas **20**, 032506 (2013).
[33]R. Hawryluk, *Physics of Plasmas Close to Thermonuclear Conditions*, edited by B. Coppi *et al.* (CEC, Brussels, 1980), Vol. 1, pp. 19–46.
[34]S. Kaye, F. Levinton, D. Stutman, K. Tritz, H. Yuh, M. Bell, R. Bell, C. Domier, D. Gates, W. Horton, J. Kim, B. LeBlanc, N. Luhmann, R. Maingi, E. Mazzucato, J. Menard, D. Mikkelsen, D. Mueller, H. Park, G. Rewoldt, S. Sabbagh, D. Smith, and W. Wang, Nucl. Fusion **47**, 499 (2007).
[35]T. Rafiq, A. H. Kritz, J. Weiland, L. Luo, and E. Schuster, Phys. Plasmas **25**, 012504 (2018).
[36]J. Candy and R. Waltz, J. Comput. Phys. **186**, 545 (2003).
[37]G. Park, C. S. Chang, I. Joseph, and R. A. Moyer, Phys. Plasmas **17**, 102503 (2010).
[38]W. Guttenfelder, J. Peterson, J. Candy, S. Kaye, Y. Ren, R. Bell, G. Hammett, B. LeBlanc, D. Mikkelsen, W. Nevins, and H. Yuh, Nucl. Fusion **53**, 093022 (2013).
[39]J. Weiland, *Stability and Transport in Magnetic Confinement Systems* (Springer, New York, Heidelberg, 2012).
[40]F. D. Halpern, G. Bateman, and A. H. Kritz, Phys. Plasmas **13**, 062510 (2006).
[41]T. Rafiq, A. H. Kritz, V. Tangri, A. Y. Pankin, I. Voitsekhovitch, and R. V. Budny, Phys. Plasmas **21**, 122505 (2014).